Small-Angle Neutron Scattering Study of Microphase Separation in Thermoassociative Copolymers

D. Hourdet,*,† F. L'alloret,†,‡ A. Durand,† F. Lafuma,† R. Audebert,† and J-P. Cotton§

Laboratoire de Physico-Chimie Macromoléculaire, Université Pierre et Marie Curie, CNRS URA 278, ESPCI, 10 rue Vauquelin, 75231 Paris Cedex, France, and Laboratoire Léon Brillouin, CEA Saclay, 91191 Gif-sur-Yvette Cedex, France

Received February 11, 1998; Revised Manuscript Received June 5, 1998

ABSTRACT: The morphology of poly(sodium acrylate)-*g*-poly(ethylene oxide) graft copolymers (PAA-*g*-PEO) in semidilute solution has been studied by small-angle neutron scattering using a temperature or salting-out effect as trigger for the phase separation of PEO side chains. As soon as the critical conditions are reached, a scattering peak arising from the correlation between the PEO domains is clearly observed. Beyond the critical conditions, e.g., at higher temperature or salt concentration, the magnitude of the fluctuations keeps on increasing while their wavelength or the periodicity of the microdomains remains constant. At the same time, the asymptotic behavior, studied at higher values of the scattering vector q, indicates that PEO side chains undergo a continuous transition from an homogeneous solution of random coils, in the weak segregation regime, to a microseparated two-phase structure with a sharp boundary in the so-called strong segregation regime (corresponding to high temperature and/or salt concentration). The modeling performed in the strong segregation regime indicates that PEO microdomains behave as polydisperse spherical micelles organized in a simple cubic lattice. Moreover, the absolute fitting of the experimental results with a polydisperse sphere model clearly indicates that the clustering of the PEO grafts, e.g., the temperature of microphase separation, the number of side chains gathered into the microdomains, and the concentration inside these clusters, is totally described, qualitatively and quantitatively, by the phase diagram of PEO. Using various copolymers, differing either by the number of hydrophilic units between the side chains (N_A) or the number of ethylene oxide units (N_B), we show that the aggregation number (N_{ag}) is mainly fixed by the primary structure of the copolymer. N_{ag} can be roughly estimated using a scaling relation taking into account its double dependence with the lengths of both hydrophilic and "hydrophobic" units: $N_{ag} \sim N_B^{\beta}/N_A^{\alpha}$.

Introduction

Microphase separation in macromolecular systems has attracted considerable interest in the field of physical chemistry of polymers mostly because this mesoscopic phenomenon provides unusual properties, in very dilute solutions (micellization of surfactants, multiblocks or telechelic polymers), concentrated media, or melts.[1−4] The common feature of all these systems is that the macroscopic properties (viscoelasticity, transparency, conductivity, etc.) can be controlled at the microscopic level by playing with the structure and the organization of the polymer chains.

In this context, water-based systems have known much development in the past decades and will be of increasing importance in the future in both society and industry. If we except the economical aspects, there are at least two basic reasons for their development. The first one is that initially water is an absolute requirement in specific fields such as food, pharmaceutical, and personal care applications. The second reason is related to problems of toxicity or more generally speaking to environment. This explains why currently water formulations tend to replace organic ones in important markets such as detergents, drilling fluids, and paints.[5] In this field, amphiphilic or hydrophobically associating water-soluble polymers have received the most attention both experimentally[6−14] and theoretically.[15−19] Basically they contain at least two types of sequences which can be included as blocks or pendant chains into the polymer structure (see Figure 1): Sequences A are purely hydrophilic. They can be neutral or ionic (+ or −) and ensure the solubility or the swelling of the copolymer in water. Sequences B are hydrophobic (alkyl, perfluoroalkyl, aromatic fragments). Their aggregation tendency (micellization) provides the amphiphilic character of the copolymer in water.

In water, these copolymers self-organize forming hydrophobic clusters embedded in a sea of hydrophilic chains. In semidilute solution, a physical network can be formed and these systems have found numerous applications as thickeners in aqueous-based fluids. In these networks, the connectivity and the lifetime of bridging units as well as the characteristics of the microdomains (size, shape, aggregation number) directly influence the viscoelastic properties of the solution. The control of the rheological properties can be regulated initially at the molecular level with the primary structure of the copolymer: the size and nature of the hydrophilic sequences; the size, nature, content, and distribution of the hydrophobic ones. Fortunately the properties of a given system are not frozen on the basis of its primary structure, and self-assembly can be modulated through external parameters playing either with the solvation strength, pH, or ionic strength[20] or favoring a synergy effect with other amphiphilic systems, surfactants, or polymers.[21−23] Moreover, with a special design of the chemical structure, associative properties can be triggered reversibly using physical stimuli such as temperature, shear stress,[24] and light.[25]

† Université Pierre et Marie Curie.
‡ Present address: Schlumberger Dowell, 26 rue de la Cavée, 92142 Clamart Cedex, France.
§ Laboratoire Léon Brillouin.

S0024-9297(98)00220-4 CCC: $15.00
Published on Web 07/24/1998

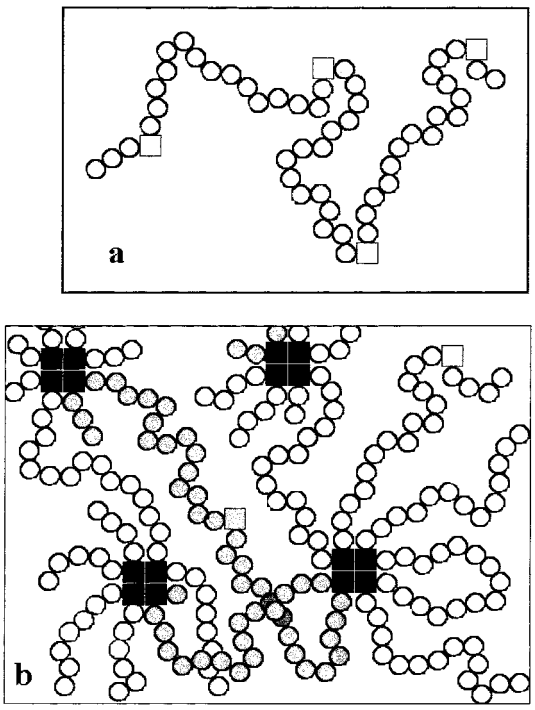

Figure 1. Schematic description of self-assembling copolymers in aqueous medium: (a) primary structure of the copolymer with short hydrophobic blocks or side chains B (□) alternating with longer hydrophilic spacers A (○); (b) physical gelation resulting from the aggregation of sequences B into hydrophobic clusters, ■ assembly.

Of course, well-known examples of gelation upon cooling were described long time ago for natural polymers such as gelatin but the opposite phenomenon, e.g., gelation upon heating, was also reported more recently in aqueous solutions. Among well-known systems, we can mention triblock copolymers of poly(ethylene oxide)-*b*-poly(propylene oxide)-*b*-poly(ethylene oxide),[26] cellulose derivatives (methyl, hydroxypropyl, and ethyl(hydroxyethyl)),[27−30] or more sophisticated systems involving mixtures of amphiphiles such as nonionic cellulose ethers and ionic surfactants[31−32] or hydrophobically modified water-soluble polymers and neutral surfactants.[33] Except for this last group, where the driving force is the phase transition of the surfactant, the gelation upon heating is generally controlled through hydrophobic interactions between the polymer chains. On this basis, we developed at the beginning of the 1990s[34] a general concept for thermoassociative polymer solutions which is based upon the switch properties of sequences B characterized by a lower critical solution temperature (LCST). Schematically, at low temperature, where both sequences A and B are soluble in water, the copolymer behaves as a classical hydrophilic system with the properties of entangled networks in semidilute solution. But now, when the temperature is increased above a critical value (T_{assoc}), the initially hydrophilic sequences B reduce their hydration by self-associating into microdomains and promote a stronger physical connectivity between the polymer chains as pictured in Figure 1. These thermoassociative systems, which possess a well-controlled primary structure, are of great interest for the following reasons:

As previously mentioned, the thermothickening is an original property compared to the thermothining behavior which characterizes most of the polymer systems or fluids in general. Like hydrophobically associating polyelectrolytes, which are often referred as antipolyelectrolyte systems (increase of the viscosity with the ionic strength in semidilute solutions), the thermoresponsive polymers could be caricatured by their anti-Arrhenius behavior.

Thermothickening, thermoviscosifying, or thermogelling is not related to a given chemical structure, but it is a general concept which was exemplified with a broad spectrum of copolymers.[35]

This property is a technological answer to a set of problems found in industrial applications where aqueous-based fluids are submitted to a heating stage during application. The control of the rheology of drilling fluids in deep subterranean formation is for instance a typical application.[36] Recently, similar systems called smart gels or intelligent gels were also depicted in popular scientific work[37] with potential applications as shoe inserts or in the medical field with drug delivery or skin care applications. Of course, in these examples, the transition temperature must be close to the body temperature.

The associating behavior is conceptually reversible, and this feature provides additional reason for technological applications where switching properties are required.

Finally, from a theoretical point of view, the switch of hydrophobic associations with the temperature provides an interesting model to follow the micellization or the aggregation of component B. As a matter of fact, one can expect to start from isolated sequences B and go, through a weak segregation regime near the critical temperature (B−B interactions being comparable to kT), toward a strong segregation regime (well above T_{assoc}) with a fairly sharp interface A/B and up to a hypothetical superstrong segregation regime.[18]

In our last papers,[35,38−40] we described the synthesis and the macroscopic properties (rheology and phase diagram) of thermothickening polymers exemplified with poly(acrylic) derivatives grafted with poly(ether) side chains.

In the present paper, we report small-angle neutron scattering (SANS) experiments performed with aqueous solutions of poly(sodium acrylate)-*g*-poly(ethylene oxide) (PAA-*g*-PEO). Using a temperature or salting-out effect as the trigger, the PEO microphase separation is studied during the different steps of aggregation. The overall set of results, obtained at the microscopic level (size, shape, concentration of the microdomains, aggregation number), is discussed in a more general context taking into account the rheological properties of the solutions and the thermodynamic behavior of the components.

Experimental Section

Materials. The synthesis and characterization of thermoassociative copolymers is described in detail elsewhere.[35] In brief, the comblike copolymers were obtained by grafting ω-methyl, α-aminopoly(ethylene oxide) (PEO) of various molecular weights on water-soluble backbones (WSB) containing a minimum amount of acrylic acid units. We generally used poly(acrylic acid) (PAA) and poly(acrylamidomethylpropanesulfonic acid-*co*-acrylic acid) (PAS-AA) with a molar composition of 80/20 for sulfonic and carboxylic functions, respectively. Depending on the solubility of the precursors, the grafting reaction was performed either in water or in *N*-methylpyrrolidone, using carbodiimide as coupling agent. The incorporation of PEO chains onto the backbone was quantitatively checked by size exclusion chromatography (SEC) during the synthesis and was confirmed by ^{1}H NMR after purification of the copolymer. For neutron scattering purposes, we have

Table 1. Primary Structure Parameters of Thermoassociative Copolymers

sample	M_{WSB}[a]	M_{PEO}[b]	τ (%)[c]	N_A[d]	N_B[e]
PAAD/0.30% PEO25	430 000[a]	28 500	0.30[c]	330	650
PAAD/0.70% PEO5	430 000[a]	6 800	0.70[c]	140	155
PAS-AA/0.55% PEO25	700 000[b]	28 500	0.55[c,d]	180	650
PAS-AA/0.50% PEO10	700 000[b]	11 600	0.50[c,d]	200	265
PAS-AA/0.60% PEO5	700 000[b]	6 800	0.60[c,d]	165	155
PAS-AA/1.35% PEO5	700 000[b]	6 800	1.35[c,d]	74	155
PAA500/0.40% PEO25	830 000[b]	28 500	0.40[c,d]	250	650
PAA500/0.40% PEO5	830 000[b]	6 800	0.40[c,d]	250	155

[a] Weight-average molecular weight of the backbone obtained by SEC (a) or light scattering (b). The polydispersity index is roughly equal to 2.5 for the different polyelectrolyte systems. [b] Viscosity-average molecular weight of PEO. The polydispersity index of the poly(ethylene oxide) chains is estimated to 1.2 from SEC. [c] Average number of PEO side chains per 100 backbone monomer units calculated from SEC (c) and/or 1H NMR (d). [d] Average number of hydrophilic units A between two PEO side chains. [e] Average number of ethylene oxide units (B) per PEO graft.

specially synthesized two samples of poly(deuterated acrylic acid)-*g*-poly(hydrogenated ethylene oxide) using the same procedure. The deuterated backbone (PAAD) was obtained by radical polymerization of acrylic acid-d_4 (Polymer Source Inc.) in deoxygenated water at pH 5 (1 mol/L). The reaction, initiated by thermal decomposition (T = 45 °C) of potassium persulfate (0.01 mol/L), was allowed to proceed for 12 h in these conditions. The crude medium was then precipitated in methanol, and the polymer was purified by several washings in pure methanol and a final drying under vacuum at room temperature. All the copolymer samples used in the present study were in the fully ionized form (Na^+ form). They are listed in Table 1.

Potassium carbonate (K_2CO_3 from Prolabo) was used as received. D_2O was purchased from Spectrométrie Spin et Techniques, and H_2O was purified with a Millipore system (Milli-RO and Milli-Q).

Sample Preparation. Polymer solutions were prepared by weighting the copolymer, the salt, and the solvent. The mixture was then put under continuous stirring at room temperature for at least 24 h to ensure complete dissolution and equilibrium of the whole system. The concentrations of the solutions are expressed, on the dry weight basis, in grams of copolymer per 100 g of solution (% w/w).

Rheology. Viscosity measurements on polymer solutions were carried out on a Carri-Med controlled stress rheometer (Rheo) with a cone/plate geometry. The Carri-Med cone calibration given by the supplier was as follows: cone diameter 2.0 cm, cone angle 2°−0−0, and truncation 55 μm.

The temperature of the measuring unit was controlled by a high-power Peltier system. Typically, the rheological analyses were performed between 20 and 75 °C in aqueous solution (isotopic mixture of D_2O/H_2O (80/20 in bulk)) with a heating rate of 2 °C/min and under constant shear rate: $\gamma = 50\ s^{-1}$.

Phase Diagrams. Phase diagrams of PEO precursors were established using turbidimetry and/or SEC. For the cloud point determination, monophasic solutions of PEO were prepared at a given concentration in H_2O with different amounts of salt (K_2CO_3). The solutions were stirred at room temperature, or below, for 24 h and then they were equilibrated in a block thermostat at a controlled temperature (ΔT = 0.2 °C). The temperature of the bath was raised by step of 1 °C every 0.5 h, and the cloud point, or temperature of phase separation T_p, was taken visually as the temperature where the samples begin to scatter visible light and thus are transformed from perfectly clear to turbid solutions. To determine the coexistence curves of the phase diagram, the PEO solutions were heated above T_p. The two phases were then allowed to settle during 48 h at a given temperature. Each phase was sampled and analyzed after suitable dilution by SEC (Waters 6000A chromatographic system equipped with four columns of Shodex OH-pak equilibrated at T = 35 °C in $LiNO_3$, 0.5 mol/L). The areas under the chromatograms, obtained by differential refractometry (Waters R401), were used to calculate the initial PEO concentration in the two separated phases, after calibration of the peak area versus PEO concentration.

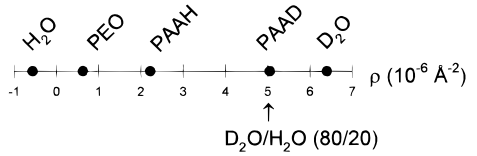

Figure 2. Scattering length densities of the different components involved in PAA-*g*-PEO aqueous solutions.

SANS. SANS experiments were performed on spectrometer PACE in the Laboratoire Léon Brillouin (CEA-Saclay, France). Two sets of experiments were carried out using an incident neutron wavelength λ = 6 and 13.9 Å with a corresponding sample−detector distance of 2.5 and 4.6 m, respectively. The scattered neutrons were collected according to scattering angles by an array of 30 circular detectors of 1 cm width. These configurations provide a scattering vector (q) ranging between 0.003 and 0.14 $Å^{-1}$. The diameter of the incident beam was 7.6 mm. The polymer solutions or the solvent was introduced into quartz cells (5 mm thick and 9 mm width) which were mounted in a temperature-controlled sample holder (precision 0.5 °C).

In the case of systems containing two types of scatterers, as in our copolymer solutions, the scattering intensity is given by the following relation:

$$I(q) \approx (\rho_2 - \rho_1)^2 v_2^2 S_{22}^T(q) + 2(\rho_2 - \rho_1)(\rho_3 - \rho_1) v_2 v_3 S_{23}^T(q) + (\rho_3 - \rho_1)^2 v_3^2 S_{33}^T(q) \quad (1)$$

where the indexes 1, 2, and 3 refer to the solvent, the PEO, and the PAAD, respectively. $S_{ij}^T(q)$ are the scattering functions; v_i is the molecular volume, ρ_i is the scattering length density, and q is the scattering vector [$q = (4\pi/\lambda)\sin(\theta/2)$] with λ the wavelength and θ the scattering angle.

For the deuterated copolymer samples, we used a solvent mixture of D_2O/H_2O, with a volume ratio of 80/20, to match the scattering length density of the PAAD backbone, $\rho_1 = \rho_3$ as shown in Figure 2. The value of this solvent ratio, initially calculated from the scattering lengths of the nuclei of the molecules and its volume, was confirmed by a contrast variation experiment with PAAD solutions using different ratios of D_2O/H_2O. Under these conditions, eq 1 reduces to its first term and all the scattering arising from the copolymer comes from the PEO grafts. For the solutions of undeuterated copolymers, the solvent used was D_2O in order to maintain a good contrast between PEO and the solvent and thus a good intensity scattered by the grafts (see Figure 2).

All data were treated according to standard procedures of small-angle isotropic scattering.[41] The spectra were corrected for transmission, sample thickness, and electronic noise. The mixture of solvents at the same composition and temperature were used as background for the samples, and the corrections for detector cell efficiency were performed by using the incoherent scattering of H_2O. The scattering intensities were converted to absolute scale using the incident neutron flux as standard. This procedure[41] allows us to give the absolute intensity $I(q)$ of eq 1 in reciprocal centimeters.

Results and Discussion

Temperature Effect. A typical thermothickening behavior in semidilute solution is shown in Figure 3 with a 2.7% solution of PAAD/0.3% PEO25 in D_2O. As defined in the Table 1, this name refers to a deuterated backbone of poly(sodium acrylate) (PAAD) carrying, per 100 backbone monomer units, 0.3 poly(ethylene oxide) side chain of ~25 000 molecular weight (PEO25).

K_2CO_3, which is characterized by a strong salting-out effect on PEO chains in water,[42] was added to the

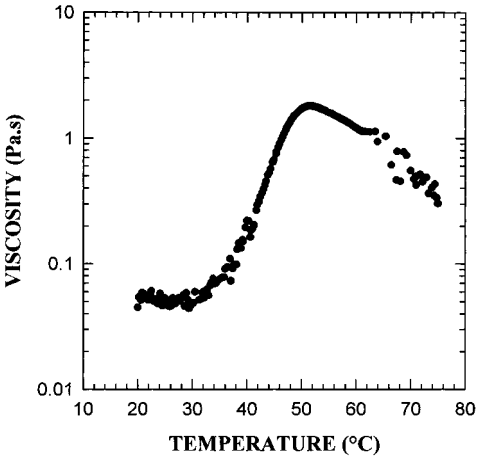

Figure 3. Typical variation of steady flow viscosity with temperature for thermoassociative copolymer solutions: sample, PAAD/0.3% PEO25; $C_p = 2.7\%$; $[K_2CO_3] = 6.9\%$; $\gamma = 50\ s^{-1}$.

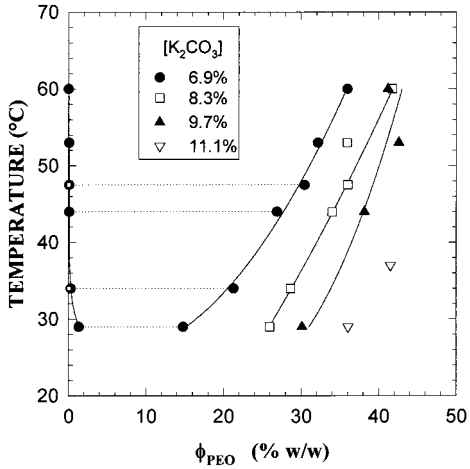

Figure 4. Phase diagram of the pseudobinary system PEO25/water for various concentrations of K_2CO_3.

solution in order to shift the transition temperature in a range compatible with our experiments, typically $T < 75$ °C. Nevertheless, from measurements performed under pressure in pure water ($T = 20-200$ °C),[40] the viscosity variation is typically the same and can be described by a two- to three-step mechanism:

(1) In the first domain, corresponding to the lower temperature range (here $T < 30$ °C), the copolymer solution behaves like a classical unassociated system. The viscosity decreases upon heating as usually observed for macromolecular solutions, organic fluids, or polymer melts, according to an Arrhenius law.

(2) From 30 to 50 °C, the viscosity increases and the magnitude of the thickening is ~1.5 decade of viscosity over $\Delta T = 20$ °C (under constant shear rate: $\gamma = 50\ s^{-1}$). The onset of the thermothickening behavior ($T_{assoc} \sim 30$ °C), which corresponds to the self-assembling of PEO grafts, is in good agreement with the value issued from the binary phase diagram of the PEO precursors in water. For instance, for the 2.7% (w/w) solution of PAAD/0.3% PEO25, the relative concentration of PEO grafts is equal to 1.3% (as the weight percentage of PEO25 in the copolymer is estimated at 48% w/w) and the corresponding phase separation of the binary PEO/water in the same conditions is $T_p \sim 29$ °C (see Figure 4). In other words, and as was previously reported,[38,40] in semidilute solutions and at copolymer concentrations that do not exceed 5% (w/w), the phase separation

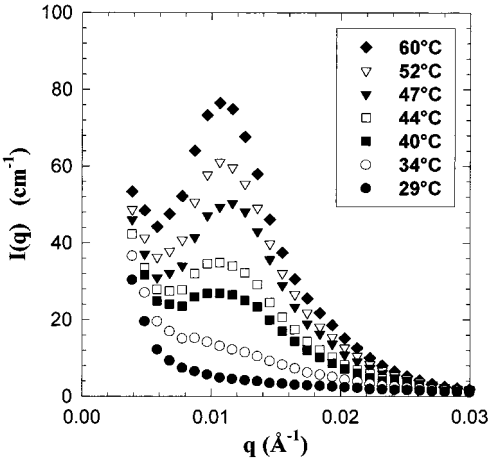

Figure 5. Variations of SANS intensities with temperature of aqueous solutions of PAAD/0.3% PEO25: $C_p = 2.7\%$; $[K_2CO_3] = 6.9\%$.

temperature of PEO remains the same whether they are grafted or free in solution.

Comparatively with similar viscometry measurements carried out in pure H_2O, we can emphasize that the deuteration labeling of the solvent has no noticeable effect on the thermodynamic behavior of these systems.

(3) Finally, the third domain observed in Figure 3 ($T > 50$ °C), characterized by a smooth decrease of viscosity upon heating, is essentially shear dependent. It results from the competition between self-assembling of PEO, promoted by heating, and stretching of supermolecular structures under shear. The resulting dynamic equilibrium, which tends to lower the connectivity of the physical network, with a probable shift from inter- to intrachains micellization, is temperature and shear rate dependent.[40] Consequently, the maximum of viscosity observed around 50 °C at a shear rate of 50 s^{-1} can be easily shifted toward lower or higher temperature by increasing or decreasing the shear rate, respectively.

We can add that the thermothickening behavior is absolutely reversible with temperature, without any hysteresis in our experimental conditions, and that the solutions remain perfectly clear on the whole range of temperature explored.

Starting from this macroscopic analogy between the thermothickening and the phase separation behavior of PEO grafts, we investigate now the microstructure using neutron scattering. Figure 5 shows the SANS data obtained, at different temperatures, with the same copolymer (PAAD/0.3% PEO25) and at the same concentrations ($C_p = 2.7\%$ and $[K_2CO_3] = 6.9\%$). As mentioned in the Experimental Section, the isotopic mixture of water ($D_2O/H_2O = 80/20$ (v/v)) is used to cancel the scattering of the PAAD backbone. At temperature below 30 °C, $I(q)$ is a monotonic decreasing function of q. However, above this temperature, $I(q)$ increases dramatically upon heating ($T = 34-60$ °C) and a scattering maximum appears and remains at a fixed position $q^* \sim 1.1 \times 10^{-2}$ Å^{-1} whatever the temperature explored above T_{assoc} is. The comparison of this scattering behavior with the phase diagram of PEO25 displays some interesting analogies which allow a qualitative description of the SANS results. At low temperature, below critical, PEO grafts behave as isolated chains in a Θ solvent. Then when the critical temperature ($T_p \sim 29$ °C) is exceeded, PEO will start to self-aggregate and give rise to concentration fluctuations

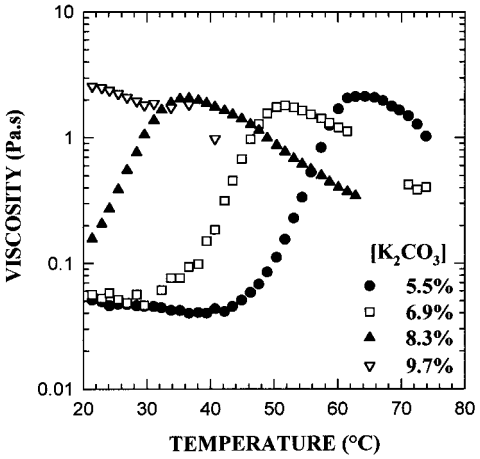

Figure 6. Influence of K_2CO_3 concentration on the thermothickening behavior of PAAD/0.3% PEO25 aqueous solutions: $C_p = 2.7\%$; $\gamma = 50\ s^{-1}$.

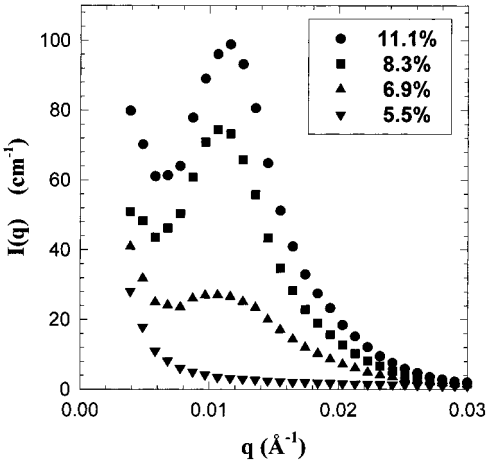

Figure 7. SANS intensities of PAAD/0.3% PEO25 aqueous solutions at various K_2CO_3 concentrations: $C_p = 2.7\%$; $T = 40$ °C.

with wavelength $2\pi/q^*$. According to the phase diagram, by increasing the temperature above T_p, both the number of PEO chains participating to the "concentrated regions" and the concentration inside the forming microdomains increase. In other words, by increasing T, we increase the magnitude of the fluctuations $\sim I(q^*)$. The fact that the position of the main peak remains constant reveals that the mean distance between the microdomains is quite independent of the temperature. The phase separation is maintained at a microscopic scale by the PAA backbones.

These results are qualitatively in agreement with those reported by Roe et al.[43] on the thermal transition in styrene−butadiene block copolymers. Using small-angle X-ray scattering (SAXS), they show that either diblock or triblock copolymers can undergo a reversible transition upon heating starting from a microdomain structure at low temperature and going toward a disordered homogeneous phase at elevated temperature. Except that the microstructural organization intervenes upon cooling, their SAXS intensity pattern is qualitatively the same. It shows (1) a gradual decrease of $I(q^*)$ upon heating and (2) a main interdomain peak at a fixed position.

Similar SANS experiments with temperature were also reported recently by Shibayama and co-workers[44−46] with poly(*N*-isopropylacrylamide-*co*-acrylic acid) copolymer solutions and gels (NIPA/AAc). For NIPA homopolymer, which is characterized by a LCST at 34 °C, the scattered intensity diverges at $q \rightarrow 0$ when approaching the transition temperature. When a few ionized groups are introduced in the NIPA chain, the critical transition is shifted toward higher temperature ($T \sim 50$ °C for NIPA/AAc 95/5 in molar ratio). Nevertheless, as soon as the temperature is raised above 34 °C, the scattered intensity is highly enhanced and a scattering maximum appears. It reveals concentration fluctuations due to the segregation between NIPA and AAc units. For linear copolymer solutions, the scattering maximum is shifted toward lower q values, when the temperature is increased in the range 34−50 °C, and a steep upturn is also observed in the low-q region. According to the authors, this behavior at low q values comes from the growing phase separation (long-range order inhomogeneities) of NIPA/AAc polymer solutions which finally reach a macroscopic demixing above 50 °C. Compared to these NIPA/AAc copolymers, we can assert that, in our systems, the macrophase separation is inhibited thanks to the large predominance of the hydrophilic component on the whole range of temperature.

Influence of Salt Concentration. By adding increasing amounts of salt into the copolymer solution, two main effects can be expected: (1) an increase of the ionic screening of the polyelectrolyte backbones and (2) an intensification of the hydrophobic character of the PEO grafts (salting-out).

From the set of experiments realized at various salt concentrations ($[K_2CO_3] = 5.5-9.7\%$ (w/w); Figure 6), one can see that salting-out prevails on the viscometric behavior. The viscosity profiles are indeed just shifted toward lower temperature, as is the cloud point of free PEO when the salt concentration increases. This macroscopic observation indicates that, in the salt range explored, the salt does not affect strongly the microstructure of the physical network, which keeps its rheological signature. This is also confirmed at the microscopic level by SANS. From experiments carried out under similar conditions ($T = 40$ °C and $[K_2CO_3] = 5.5-11.1\%$ (w/w); Figure 7) we can see that the scattering peak is always centered on the same position ($q^* \sim 1.05 \times 10^{-2}$ Å^{-1}). This is true at $T = 40$ °C, but of course the same holds at higher temperature as previously reported. In other words, the mean distance between the microdomains remains constant in all the salinity range explored. In that case, we conclude that the organization of the physical network depends only on the primary structure of the copolymer. Another interesting feature concerns the magnitude of these concentration fluctuations. As previously seen, $I(q)$ initially starts to increase dramatically as soon as the critical temperature is reached. Then the scattering intensity keeps on increasing with salt or temperature and finally reaches a plateau around $I(q^*) = 100-120$ cm^{-1} at high temperature and/or K_2CO_3 concentrations ($T = 40$ °C and $[K_2CO_3] = 11.1\%$ (w/w), $T = 57.5$ °C and $[K_2CO_3] = 8.3-9.7\%$ (w/w)). This phenomenon cannot be attributed to the contrast due to the presence of salt in water as salt only leads to negligible variation. Again, this feature can be best compared to the solubility gap of PEO25 (see Figure 4) where the concentrated phase reaches some limiting value around 40% (w/w) at high temperature and/or K_2CO_3 concentrations.

Influence of the Copolymer Concentration. The viscosity/temperature profile of PAAD/0.3% PEO25

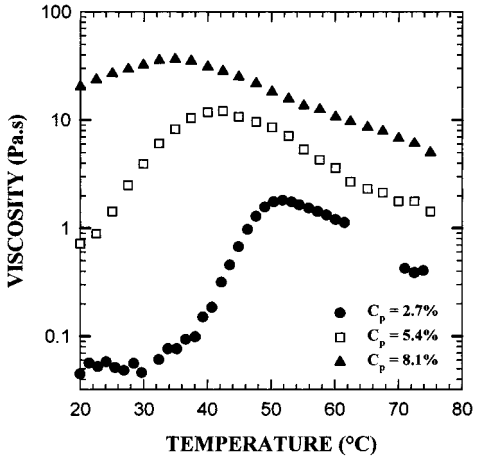

Figure 8. Influence of the copolymer concentration on the rheological behavior of PAAD/0.3% PEO25 aqueous solutions: $[K_2CO_3] = 6.9\%$; $\gamma = 50\ s^{-1}$.

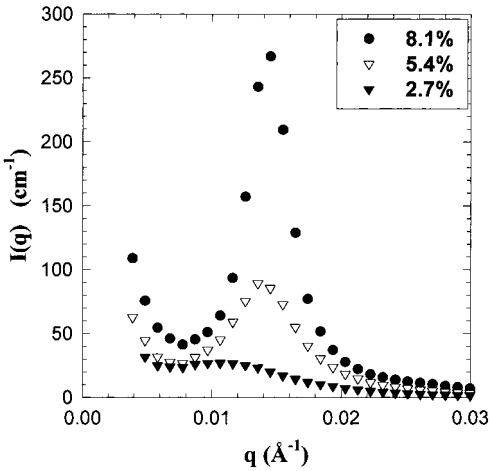

Figure 9. Variations of SANS intensities with copolymer concentration: sample, PAAD/0.3% PEO25; $[K_2CO_3] = 6.9\%$; $T = 40$ °C; C_p are assigned inside the figure.

aqueous solutions was recorded at constant salt concentration ($[K_2CO_3] = 6.9\%$ (w/w)) for various copolymer concentrations (Figure 8). As expected, we observe a dramatic enhancement of the viscosity with the concentration as a result of the increasing number of intermolecular physical cross-links (or elastically active chains). At the same time, the association temperature is shifted toward lower temperature as is the cloud point of PEO (see Figure 4). Nevertheless, the relative increase of PEO content is not the only reason, and at high copolymer concentration (above 5% (w/w)) it is necessary to take into account the increasing concentration of poly(sodium acrylate), which favors the self-assembling of PEO at lower temperature, as in the ternary diagram PAA/PEO/H_2O ($[K_2CO_3] = 6.9\%$ (w/w)).

The corresponding SANS data, obtained in similar conditions ($[K_2CO_3] = 6.9\%$ (w/w) and $T = 40$ °C), are reported on Figure 9. For $C_p = 2.7\%$ (w/w), we are very close to the transition (weak segregation regime) and the scattering intensities remain very low with a slight scattering maximum ($q^* \sim 1.05 \times 10^{-2}$ Å^{-1}) flattened out on that scale. By raising the copolymer concentration from 2.7 to 5.4% and finally up to 8.1%, the scattered intensity increases rapidly while the peak position moves toward higher q values: 1.35×10^{-2} and 1.45×10^{-2} Å^{-1} for $C_p = 5.4$ and 8.1%, respectively. If the position of the peak is taken as a measure of the most probable distance d between the aggregates, then we obtain $d = 2\pi/q^*$ equal to 590, 465, and 435 Å for copolymer solutions at 2.7, 5.4, and 8.1%, respectively. These mean interaggregate distances can be scaled with the copolymer concentration (or the relative PEO concentration) according to $d \sim C_p^{-0.3}$. In our experiments, performed at relatively high ionic strength ($[K_2CO_3] = 5.5-11.1\%$ (w/w)), this scattering behavior with an exponent close to $-1/3$ can be attributed unambiguously to an isotropically dilution process of scattering objects of given size and not to a polyelectrolyte effect as reported with various water-soluble systems.

For instance, in the case of weakly charged polyelectrolytes in poor solvent,[44,46,47] a microscopic phase separation takes place as a compromise between (1) attractive forces originating from "hydrophobic" backbones and (2) repulsive electrostatic interactions which result from the charged groups. Consequently, for these systems, the scattering peak that appears near the Θ temperature of the backbone can be shifted toward smaller q values not only by decreasing the polymer concentration but also by increasing the ionic strength or reducing the ionization degree. In the case of NIPA/AAc gels in pure water and at $T = 46$ °C, Shibayama et al.[44] showed that the main interdomain distance d can be roughly scaled with the polymer volume fraction with an exponent closer to $-1/4$ (rather than $-1/3$) as predicted by Borue and Erukhimovich[48] in their statistical theory for polyelectrolyte in poor solvent.

At the opposite, for highly charged polyelectrolyte in water, a broad scattering peak is generally observed as a result of the correlation hole effect around the chains promoted by electrostatic repulsions.[49] In that case, the scaling dependence between d and C_p was predicted with a theoretical exponent of -0.5. Experimentally, with poly(sodium styrenesulfonate), the exponent was found to vary between -0.4 and -0.5 when the degree of sulfonation increased from 35 to 87% (in moles), respectively.[50]

From this first set of experiments we can see that the thermoassociative behavior of the copolymers, which proceeds through a microphase separation mechanism, can be qualitatively pictured on the basis of the thermodynamic properties of the PEO grafts. Moreover, it seems that the characteristic parameters of the forming microdomains are directly connected with the primary structure of the graft copolymers. In the following part of this paper, we will try to investigate more quantitatively this microphase separation process and the characteristics of the resulting micelles (size, shape, number of aggregation).

Asymptotic Behavior. To obtain a quantitative or at least a more accurate picture of the microdomain formed upon heating, the initial set of experiments was extended at higher q values ($0.02 < q < 0.13$ Å^{-1}). A log−log plot of $I(q)$ versus q is given in Figure 10 for PAAD/0.3% PEO25 solutions ($C_p = 2.7\%$) measured at various potassium carbonate concentrations and/or temperatures. As we increase the temperature and/or K_2CO_3 concentration, the asymptotic behavior of the scattered intensity also changes systematically according to $I(q) \sim q^{-\mu}$. The exponent μ is related to the balance between attractions and repulsions inside the polymer chain.[41] If the polymer segments repel each other, as for polymers in good solvent, $\mu < 2$ is expected with critical values of $5/3$ corresponding to self-avoiding walk (excluded-volume effect) and $\mu = 1$ for rigid rods.

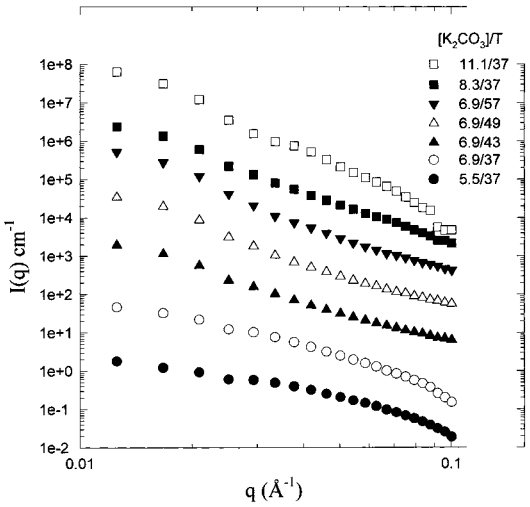

Figure 10. SANS intensity behavior of PAAD/0.3% PEO25 aqueous solutions in the intermediate q range. The enclosed x/y values refer to "K_2CO_3 concentration (% w/w)/temperature" conditions experienced for each solutions. Starting from the lower curve (5.5/37), plotted in absolute scale, the following curves are each displaced from the preceding one by a factor of 10 along the y-axis in order to avoid overlapping.

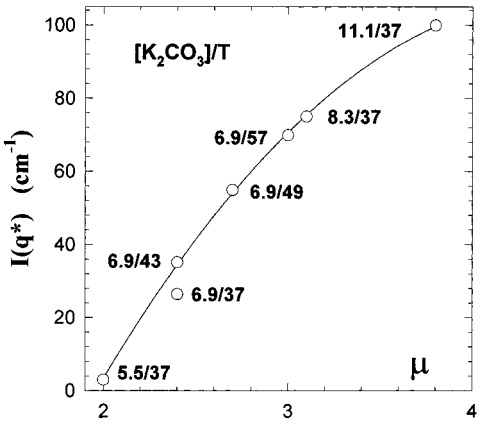

Figure 11. SANS intensities at q^* as a function of the scattering exponent calculated from the asymptotic behavior reported on Figure 10. The x/y values correspond to the K_2CO_3 concentration/temperature conditions: sample, PAAD/0.3% PEO25; $C_p = 2.7\%$.

If the segments attract each other in the solvent, as for collapsed polymer coils, $\mu > 2$. When this force vanishes, for Gaussian configuration for instance (random coil), $\mu = 2$.

The values of μ were calculated in our systems from the slope of the curves plotted on Figure 10 for q values ranging between 0.03 and 0.1 $Å^{-1}$. Due to the low scattering intensities obtained at the highest values of q, the determination of the absolute values of $I(q)$ is very sensitive to the subtraction of the solvent intensity used as a reference. Consequently, μ values are given within a gap of $\pm 0.1-0.2$. To give an overall description of the microphase separation, we plot in Figure 11 the scattering intensities at q^* versus μ. As previously depicted, we can see that $I(q^*)$, which is related to the microdomain formation, increases continuously when either the temperature or the salt concentration is raised. According to the previous set of experiments, a plateau seems to be reached at high level of phase separation, around $I(q^*) \sim 100-120$ cm^{-1}. The same consideration also holds for μ values. For the copolymer solution just below the critical conditions of phase separation (i.e., $[K_2CO_3] = 5.5\%$, $T = 37$ °C; see Figure 5), the critical exponent is equal to 2 as expected in the θ region. Then by increasing the aforementioned parameters (T or $[K_2CO_3]$), μ continuously increases and approaches 4 as $I(q^*)$ reaches its "limiting" value. This scattering exponent of 4 indicates that the scattering pattern corresponds to a microseparated two-phase structure with a sharp boundary according to the so-called Porod law.[51] Moreover, it definitively discriminates this mechanism from a possible "correlation hole" effect which could be expected with block copolymers when the concentration fluctuations are large enough.

If we come back to the phase diagram of PEO given in Figure 4, we can see now that the self-assembling, enlightened by SANS, proceeds in a similar way. Moreover by studying the temperature-induced association in grafted PEO systems, we obtain additional information as the different thermodynamic steps of the phase separation are "frozen" at the microscopic scale.

(1) In salt/temperature conditions well below critical, the PEO grafts are quite soluble in aqueous medium and a self-avoiding walk can be expected, at least for long chains. The whole copolymer solution behaves as a homogeneous system close to the one obtained under the same conditions with the water-soluble backbone.

(2) By increasing salt concentration or temperature, the excluded volume of PEO vanishes and the graft conformation becomes Gaussian near the θ point (close to the solubility gap).

(3) When entering into this latter stage, PEO start to self-aggregate (weak segregation regime). We have no information about the mechanism of phase separation (nucleation and growth or spinodal decomposition), but the microdomain formation (size and shape) is basically controlled by the primary structure of the copolymer in order to minimize the micellar free energy F which takes into account the contributions originating from the core (F_{core}), the corona (F_{corona}) and the interface (F_{int}).[18]

(4) As we go upward in the solubility gap, the number of PEO participating in the microdomains and the concentration inside these clusters increase. In accordance with the phase diagram of PEO, we observe by SANS an increase of both the scattering intensity $I(q)$ and the exponent μ. At a high level of phase separation (high T or C_s), the system reaches a strong segregation regime where all the PEO grafts are embodied into clusters having a sharp interface. According to SANS, the copolymer seems to have reached at this point a given equilibrium which remains unaltered, in our experimental conditions, by still increasing temperature or salt concentration. This macroscopic behavior is in good agreement with the phase diagram of PEO where two limiting values, corresponding to $\phi_{PEO} \sim 0$ and 40% (w/w), were obtained for dilute and concentrated phases, respectively (see Figure 4). Nevertheless, it is worthwhile to mention that these so-called limiting values are relative to the temperature/salt conditions explored in our experiments. Of course we do not expect that these limits remain unchanged indefinitely and especially at very high temperature. As PEO is known to undergo an UCST-type phase transition at elevated temperature, a dissolution of PEO aggregates can be predicted at very high temperature, but this is out of the scope of the present paper.

Microdomains Characterization. Radius of the Micelles. In this section, we will take advantage of the

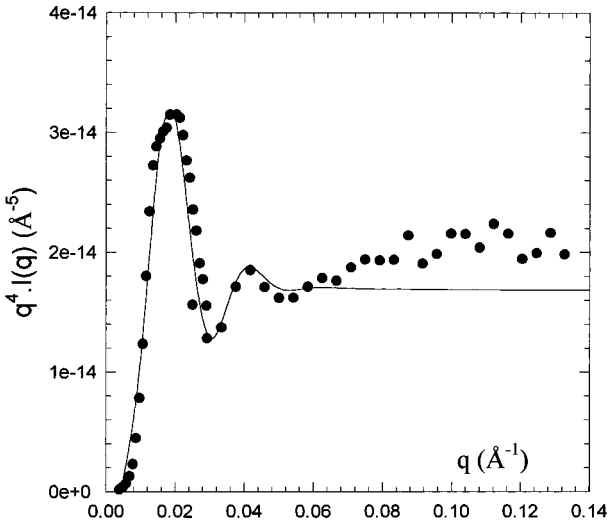

Figure 12. Modeling of the SANS behavior of thermoassociative copolymer solution in the strong aggregation regime. (●) Experimental data obtained with an aqueous solution of PAAD/0.3% PEO25: $C_p = 2.7\%$; $[K_2CO_3] = 11.1\%$; $T = 37$ °C. (−) Theoretical curve corresponding to the model of polydisperse spheres. The best fit is obtained using an average radius $R = 132$ Å, a standard deviation $\sigma = 28$ Å, and an adjusting parameter $Z_{fit} = 1.12 \times 10^{-13}$ Å^{-4}.

aforementioned results, exploring the situation where a strong segregation regime is reached (high temperature and/or salt concentration). For all the morphologies corresponding to that state, we assume complete phase separation and negligible interface thickness, which seems a reasonable assumption as evidenced by the q^{-4} dependence of the scattering intensity. Schematically, the solution can be sketched by spherical micelles ("PEO + water") embedded regularly into a continuous salted aqueous solution of poly(sodium acrylate) backbone. Moreover, to fulfill the picture issued from the q^{-4} dependence (sharp interface and no fluctuation of concentration inside the hydrated core of the micelle), we must consider that "PEO + water" forms, inside the microdomains, a stable hydrated complex. This idea is, of course, well supported by the large number of papers which deal with hydration complexes, mostly ranging between two and three molecules of water per ethylene oxide unit.[52−56]

The assumption of a strong segregation regime can be simply tested, using the scattering data obtained at $[K_2CO_3] = 11.1\%$ and $T = 37$ °C (see Figure 12), by comparing the experimental and theoretical values of the so-called invariant Q_{exp} and Q_{th}, respectively. The invariant values are calculated from the following relations:

$$Q_{exp} = \int_0^\infty q^2 I(q)\, dq \tag{2}$$

and

$$Q_{th} = 2\pi^2(\rho_1 - \rho_2)^2\phi_1\phi_2 \tag{3}$$

where ρ_1 and ρ_2 are the scattering length densities of the two phases (1 refers to PAAD phase and 2 to PEO micelles). ϕ_1 and ϕ_2 are the volume fractions of the two phases.

Q_{exp} can be obtained by integrating the experimental values plotted as $q^2I(q)$ vs q:

$$Q_{exp} = 2.26 \times 10^{-12}\ \text{Å}^{-4}$$

For the determination of Q_{th} we used our experimental data issued from the phase diagram of PEO (see Figure 4) and the scattering length densities of the components. The calculated parameters are as follows: (1) $\phi_{PEO} = 0.014$, the volume fraction of pure PEO in the whole solution; (2) $\phi_2 = 0.034$ ($\phi_1 = 1 - \phi_2 = 0.966$), the volume fraction of PEO micelles in the whole bulk, assuming a volume fraction $X_{PEO} = 0.41$ (see Figure 4) for PEO inside the micelles; (3) $\rho_1 = \rho_{D_2O/H_2O} = 5 \times 10^{-6}$ Å^{-2}; and (4) $\rho_2 = X_{PEO}\rho_{PEO} + (1 - X_{PEO})\rho_{D_2O/H_2O} = 3.21 \times 10^{-6}$ Å^{-2}, where ρ_{PEO} is the scattering length density calculated for pure PEO ($\rho_{PEO} = 0.63 \times 10^{-6}$ Å^{-2}; see Figure 2) and ρ_{D_2O/H_2O} is the one calculated for the solvent mixture D_2O/H_2O (80/20 v/v) as the K_2CO_3 contribution is negligible in our conditions.

Basically the determination of values lies on a single liquid approximation, e.g., assuming that the solvent ratio D_2O/H_2O is the same inside and outside the micelles. From these calculated parameters we obtain a theoretical value $Q_{th} = 2.08 \times 10^{-12}$ Å^{-4} in good agreement with the experimental one.

This intermediate result provides a self-consistent check of the aforementioned hypotheses: (1) Validity of the two phases model; (2) estimation of ϕ_i and ρ_i values from the pseudobinary phase diagram of PEO. The next step is then the determination of the specific area of the particles using the Porod limit:

$$\frac{S}{V} = \frac{\pi\phi_1\phi_2}{Q}\lim_{q\to\infty} I(q)q^4 \tag{4}$$

where S is the total interface area in the scattering volume V, the other parameters being previously defined.

Assuming spherical micelles, we obtain an average core radius $R_{core} = 112$ Å according to

$$R_{core} = \frac{3}{\pi\phi_1}\frac{Q}{\lim q^4 I(q)} \tag{5}$$

and using $Q_{exp} = 2.26 \times 10^{-12}$ Å^{-4} and $\lim q^4I(q) = 2 \times 10^{-14}$ Å^{-5} (see Figure 12).

Note that the core radius obtained according to eq 5 is roughly independent of any phase diagram assumption as $\phi_1 \sim 1$.

The average core radius can also be calculated using two other independent methods.

The simplest one only considers the average intermicellar distance ($d = 2\pi/q^*$) and the volume fraction of PEO micelles (ϕ_2), according to the following relation:

$$R = \left(\frac{3}{4\pi}\right)^{1/3}\phi_2^{1/3}\alpha^{1/3}d \tag{6}$$

The parameter α in relation 6 depends on the organization of the spherical microdomains. Three regular lattice types are assumed: (1) simple cubic (SC with $\alpha = 1$), body-centered cubic (BCC with $\alpha = 4/3^{3/2}$) and face-centered cubic (FCC with $\alpha = 1/2^{1/2}$).

Using the experimental values $d = 590$ Å and $\phi_2 = 0.034$, we obtain

$$R_{SC} = 119\ \text{Å} \qquad R_{BCC} = 109\ \text{Å} \qquad R_{FCC} = 106\ \text{Å}$$

We can see that whatever the lattice type is, the micellar

radii obtained $R = 105-120$ Å are in good agreement with the value calculated from the Porod limit, $R_{core} = 112$ Å.

The second method used here, allows a more precise determination of the shape of the scattering particles by fitting the experimental results with an appropriate model. Basically, for spherical particles (index 2) embedded regularly in a continuous medium (index 1), the absolute scattering intensity (first term of eq 1) can be written as

$$I(q) = (N_p v/V)\phi_1(\rho_1 - \rho_2)^2 F(q)S(q) \quad (7)$$

where ϕ_1 and ϕ_2 ($\phi_2 = N_p v/V$) are the volume fractions of the two phases as previously defined, N_p is the number of spherical particles of volume v (radius r) in the whole scattering volume V, ρ_1 and ρ_2 are the scattering length densities, $F(q)$ is the form factor, which contains the information about the size and shape of the particles, and $S(q)$ is the structure factor for the correlation between the particles. In the asymptotic q range ($qr > 1$), corresponding here to $q > 0.01$ Å^{-1} for $r \sim 100$ Å, we will consider that the scattering is dominated by the form factor ($\rightarrow S(q) \sim 1$).

In Figure 12, the scattering data corresponding to the sample PAAD/0.3% PEO25 ($C_p = 2.7\%$, $[K_2CO_3] = 11.1\%$, and $T = 37$ °C) were plotted according to $q^4 I(q)$ vs q. This representation clearly evidences the damped oscillations of $I(q)$ which superimposed the q^{-4} dependence. This indicates either that the domains are not spherical or that there is some size polydispersity, but it is not possible to differentiate between the two effects. In the following, we consider that the PEO micelle solution behaves as a polydisperse solution of homogeneous spheres with a Gaussian size distribution. In that case, for a sphere of volume

$$v = ({}^4/_3)\pi r^3 \quad (8)$$

the form factor is given by

$$F(q) = \int_{-\infty}^{+\infty} v[\psi(q,r)]^2 \omega(r)\, dr \quad (9)$$

with

$$\psi(q,r) = 3\,\frac{\sin(qr) - qr\cos qr}{(qr)^3} \quad (10)$$

and

$$\omega(r) = \frac{1}{(2\pi)^{1/2}\sigma}\exp\left(-\frac{(r-R)^2}{2\sigma^2}\right) \quad (11)$$

$\omega(r)$ is the Gaussian function for the distribution of sphere radius, with R the average radius and σ the standard deviation.

According to this model, the best fit gives an average radius: $R = 132$ Å and a standard deviation $\sigma = 28$ Å. Although a similar fit could be realized using the form factor calculated from a solution of monodisperse ellipsoids, we consider that the good agreement obtained here, between the average radius issued from this simulation and the other values calculated independently ($R = 105-120$ Å), is consistent with the spherical shape of PEO micelles. Moreover, according to this spherical model, a closer comparison between the values obtained from space-filling calculations ($R_{SC} = 119$ Å, $R_{BCC} = 109$ Å, $R_{FCC} = 106$ Å) tends to favor the simple cubic lattice for the PEO microdomains.

One additional piece of information can be obtained from this simulation if we take into account the adjusting parameter used to superimpose the theoretical curve and the experimental one. Starting from eq 7, and assuming as already mentioned that $S(q) \sim 1$, we can see that the scattering intensity varies linearly with the form factor according to

$$I(q) = ZF(q) \quad (12)$$

with

$$Z = \phi_1\phi_2(\rho_1 - \rho_2)^2 \quad (13)$$

Using the following values ($\phi_2 = 0.034$, $\phi_1 = 1 - \phi_2$, $\Delta\rho^2 = 3.20 \times 10^{-12}$ Å^{-4}), mostly issued from the phase diagram of free PEO, we obtain a calculated value $Z_{cal} = 1.05 \times 10^{-13}$ Å^{-4}, which has to be compared to the fitting parameter $Z_{fit} = 1.12 \times 10^{-13}$ Å^{-4}. Once again, the good agreement obtained here strengthens the comparison between macro- and microphase separation. The important conclusion is that the associative behavior of WSB-*g*-PEO systems can be controlled on the basis of the thermodynamic properties of PEO grafts. Indeed, the critical conditions of self-association (T or C_s), the fraction of PEO grafts gathered into the microdomains, and the concentration of the microdomains are perfectly described by the phase diagram of PEO precursors. Moreover, we can add that the volume fraction of PEO inside the microdomains, $X_{PEO} = 0.41$ as determined in the strong segregation regime, agrees fairly well with the value calculated on the basis of a "$3H_2O$/1EO" complex ($X_{PEO} \sim 0.42$).

Nevertheless, even if the PEO side chains are the trigger of this mechanism, we must consider also the interplay of the water-soluble backbone in the microdomain formation, specially because it stabilizes the PEO phase at the nanoscopic level. If we consider the problem of self-assembling from this point of view, a question immediately rises: What is the relation between the primary structure of the copolymer and the characteristics of the microdomains?

Average Number of Aggregation. In this last part, the SANS study was extended to all the samples listed in Table 1. As previously reported, most of them are hydrogenated and were studied in pure D_2O. The scattering intensity follows eq 1. Although the polyelectrolyte backbone was not matched by the solvent in these conditions, the scattering curves always displayed a main diffraction peak which was assigned to the average interaggregate distance. From these distances, an average aggregation number (N_{ag}) was calculated by assuming the following: (1) that all the PEO grafts are embedded into the microdomains. As previously depicted, this is only true in the strong segregation regime (high T or C_s), but as the interaggregate distance remains constant during the association process, this hypothesis holds for the extrapolation of N_{ag} in the strong segregation regime; (2) that the PEO micelles are organized into a SC lattice which gave the best agreement between fitting and space-filling calculations.

For this set of samples, the average number of aggregation reported in Table 2 was calculated according to the relation

$$N_{ag} = A_{vo}(m_{PEO}/M_{PEO})d^3 \quad (14)$$

Table 2. Primary Structure of Copolymers and Aggregation Parameters Issued from SANS Studies Performed in Aqueous Solution

sample	C_p (%)[a]	C_s (%)[a]	T (°C)[a]	d (Å)[b]	N_A[c]	N_B[c]	N_{ag}[d]
PAAD/0.7% PEO5	3	9.7	>45	360	140	155	38 ± 3
PAA500/0.4% PEO5	3	13.8	60	460	250	155	47 ± 5
AMPS-AA/0.6% PEO5	9	16.6	20	380	165	155	64 ± 6
AMPS-AA/1.35% PEO5	9	13.8	60	340	74	155	92 ± 8
AMPS-AA/0.5% PEO10	3	13.8	60	650	200	265	85 ± 13
AMPS-AA/0.55% PEO25	3	8.3	60	720	180	650	94 ± 16
PAA500/0.4% PEO25	3	6.9	60	650	250	650	78 ± 12
PAAD/0.3% PEO25	3	> 6.9	> 20	590	333	650	56 ± 7

[a] These are the conditions of SANS experiments, where C_p, C_s, and T are the copolymer concentration, the K_2CO_3 concentration, and the temperature, respectively. [b] $d = 2\pi/q^*$ is the intermicellar distance obtained from the maximum of the SANS intensity profile. [c] N_A and N_B, previously defined in Table 1, are the average numbers of monomer units in hydrophilic and LCST sequences, respectively. [d] N_{ag} is the aggregation number calculated from eq 14.

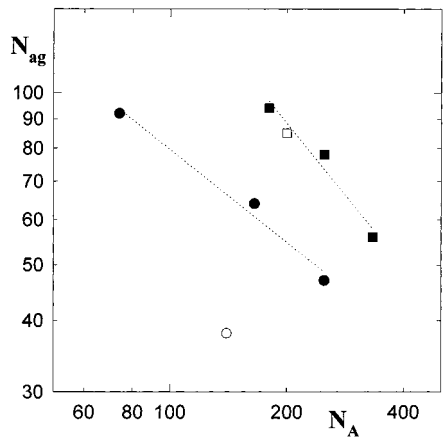

Figure 13. Double-logarithmic plot of the experimental aggregation number (N_{ag}) versus the hydrophilic block length (N_A). The following symbols refer to the thermoassociative systems detailed in Table 2: (■) WSB-*g*-PEO25; (□) WSB-*g*-PEO10; (●) WSB-*g*-PEO5 studied at $[K_2CO_3] = 13.8-16.6\%$; (○) WSB-*g*-PEO5 studied at $[K_2CO_3] = 9.7\%$.

with m_{PEO} the weight (g) of PEO per 1 mL of solution, M_{PEO} the molar mass of the PEO chain, A_{vo} the Avogadro number, and d the intermicellar distance estimated from q^*.

From these results, it appears that the aggregation number is not simply dominated by one of the two components A or B. At constant PEO block length (N_B), for instance, the aggregation number decreases when the length of the hydrophilic spacer (N_A) increases. At the opposite, the aggregation number scales positively with the PEO block length. This can be more easily shown by plotting under logarithmic scale N_{ag} versus N_A (Figure 13). Roughly, two linear relations can be obtained, taking separately

the PEO25 series studied at medium salt concentration: $[K_2CO_3] = 6.9-11.1\%$

$$N_{ag} \sim N_B^{\beta}/N_A^{\alpha} = 3600/N_A^{0.7} \qquad (15)$$

the PEO5 series studied at high salt concentration: $[K_2CO_3] = 13.8-16.6\%$

$$N_{ag} \sim N_B^{\beta}/N_A^{\alpha} = 1000/N_A^{0.54} \qquad (16)$$

Here, these two relations clearly exhibit that the aggregation number always decreases when the water-soluble block length increases. This seems a general rule even if the slopes of the relations are different. If we focus on the PEO5 series, we can see that the PAAD/PEO5 sample, which is the only one studied at lower salt concentration ($[K_2CO_3] = 9.7\%$), does not scale with the three other PEO5 copolymers (see Figure 13). An unexpected very low value of the aggregation number is obtained in that case ($N_{ag} = 38$). One way to understand this discrepancy in the PEO5 series is to take into account the salt concentration as a pseudo-variable. In the following section, we will consider that the salt concentration, or the ionic strength, influences the swelling of the backbone and modifies, consequently, the interfacial properties. We assume that this phenomenon, which is responsible for the backbone shrinking, is especially enhanced at high salt concentration. For simplicity we identify, independently of the PEO grafted copolymers, two ranges of salt concentration characterized by a constant value:

for $[K_2CO_3] < 12\%$, $\alpha = 0.70$ for $[K_2CO_3] > 12\%$, $\alpha = 0.54$

Of course α could be considered as a simple adjusting parameter, but the two reported values are not meaningless. They reveal some information about the swelling/collapse behavior of the WSB backbone as does, for instance, the Mark−Houwink coefficient in the intrinsic viscosity/molar mass relation. The physical meaning of α can be more easily understood using simple considerations about micelle formation. Whether low-molecular-weight surfactants or multiblock copolymers are considered, the micellization arises from three main contributions:[57] (1) The driving force for micelle formation is provided by the free energy of transfer of the insoluble component B from the initial solution to the micellar core. (2) The cooperative growth of surfactant micelles is promoted by the free energy term accounting for the formation of the core/corona interface (B/A). (3) The third contribution is the anticooperative inhibition of micellar growth, which can be related to steric and/or electrostatic repulsions experienced by the soluble segments A in the corona.

Using this simple description, we can see that every modification that decreases the repulsive interactions between the A blocks will favor an increase of the aggregation number, decreasing in the same way the interface area. In water-based systems such as ours, this can be obtained by increasing salt concentration, for instance, playing with the Flory−Huggins interaction parameter between the soluble A-block and the solvent (χ_{AS}). Following this argument and decreasing continuously the solvent quality for A segments, one can easily imagine that the inhibition of micellar growth will vanish beyond some given value of χ_{AS}, giving rise to a macrophase separation.

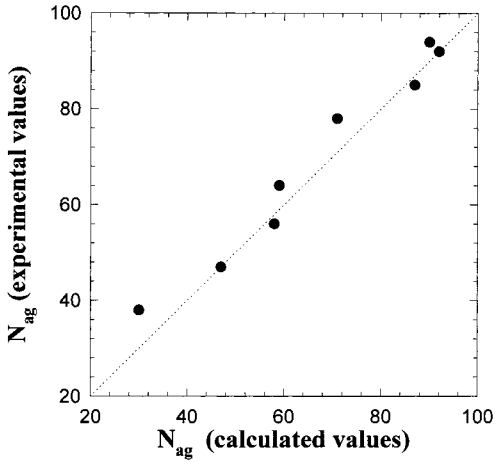

Figure 14. Comparison between experimental aggregation numbers and calculated values issued from relation 17.

Coming back to our copolymer, and taking into account the three above-mentioned variables, N_A, N_B, and α, the micellization behavior of all the systems investigated can be depicted by a single relation:

$$N_{ag} = 10N_B^{0.9}/N_A^{\alpha} \tag{17}$$

with α (equal to 0.54 or 0.70) the pseudovariable previously defined.

The aggregation numbers calculated according to this equation and the experimental values are compared on Figure 14. The good agreement obtained here gives consistency to this three-parameter equation. Furthermore, we must add that this dependence of N_{ag} on N_A and N_B does not lie on the initial assumption of a simple cubic lattice structure as the same qualitative relation could be obtained using a bcc lattice for instance.

As previously mentioned, we observe an increase of N_{ag} with the length of the insoluble block ($N_{ag} \sim N_B^{\beta}$). This general behavior has been reported with most of the systems that self-assemble in selective solvents, either diblocks or triblocks. By the way, various theoretical treatments,[58−61] based on block copolymer micellization, give a scaling relation of the following type:

$$N_{ag} \sim N_B^{\beta} \tag{18}$$

with numerical β values varying between 0.5 and 1 depending on the block length ratio N_A/N_B and the strength of the interfacial energy.

According to relation 18, the solvent-compatible block is considered to have no influence on the micellar characteristics, either N_{ag} or Rcore. Nevertheless, we can find some other examples where the soluble block has been reported to have some reasonable effect on the micellization. This is the case for block copolymer self-assembly in selective solvents such as poly(styrene)-*b*-poly(isoprene) in heptane[57,62] or poly(styrene)-*b*-poly(sodium acrylate) in water.[63] Moreover, unlike the above-mentioned theoretical treatments, Nagarajan and Ganesh[57] have proposed another thermodynamic approach for the micellization of AB diblock copolymer molecules in a selective solvent. Note that this treatment was also extended further to BAB triblocks.[64] In contrast to the predictions of the earlier models, their theory reveals that the solvent-compatible shell block A can have a strong influence on the micellar properties, depending on the nature of its interactions with the solvent. Clearly that means that both the soluble block length N_A and the interaction parameter χ_{AS} have to be taken into account for the description of the micelle characteristics. In their modeling based upon experimental data, they show that the soluble blocks A become relatively more prominent in systems where the solvent is very good for A. For example, with poly(A)-*b*-poly(B)/solvent systems at $T = 25$ °C such as PEO-*b*-PPO/water ($\chi_{AS} = 0.2$) or poly(butadiene)-*b*-poly(styrene)/heptane ($\chi_{AS} = 0.5$), they obtain respectively

$$N_{ag} \sim N_B^{1.19}/N_A^{0.51} \qquad \text{and} \qquad N_{ag} \sim N_B^{1.10}/N_A^{0.24} \tag{19}$$

Finally, these observations concerning the influence of block A on the micellization, which are evidenced in the eqs 17 and 19, were also mentioned in the theoretical treatment of polysoap micelles.[16] For instance, when compared to free surfactants, the corona free-energy contribution involved in polysoap micellization increases with the length of the spacer chains between linked surfactants (N_A). The resulting contribution is then a decrease of the aggregation number, which could be repressed ($N_{ag} \sim 1$) for very large values of N_A.

Conclusions

From a wide set of macroscopic experiments performed on PEO grafted copolymers in aqueous solution, and completed here at the microscopic scale by SANS, we are now able to give a quasi-quantitative picture of the phase separation process induced by heating. For this purpose we can separate arbitrarily the two relevant parameters, which are the structure of the copolymer and the thermodynamic properties of its components.

First, using various copolymer samples, we have found that the architecture has direct implications on the characteristics of the microdomains and especially on the aggregation number. Without any thermodynamic consideration, we can state that N_{ag} is mainly controlled by the primary structure of the macromolecular system. In the case of grafted copolymers, this can be realized during the synthesis by adjusting the structural parameters N_A and N_B, playing with the size of the PEO grafts, the grafting ratio, or the distribution of the PEO side chains along the water-soluble backbone. Every increase of N_B or decrease of N_A will increase the aggregation number of the microdomains if the structures are compared in similar conditions.

Besides this structural feature, the most important aspects arising from the present study are the thermodynamic properties of the components of the copolymer which can be described through the Flory−Huggins interaction parameters (χ_{BS}, χ_{AS}, χ_{AB}).

χ_{BS}, which corresponds to the PEO/water system, has been extensively discussed throughout this work, especially because its variation with temperature is the trigger of the self-assembling process. The comparison between SANS performed on PEO grafted copolymers and the phase diagram of free PEO in aqueous solution has revealed the close resemblance between the two mechanisms. The conclusion that can be drawn is that, in the conditions experienced here and especially in the low copolymer concentration range, the phase-separation process of PEO proceeds indifferent to whether they are free in solution or linked at one end to the water-soluble backbone. More precisely, we can consider that

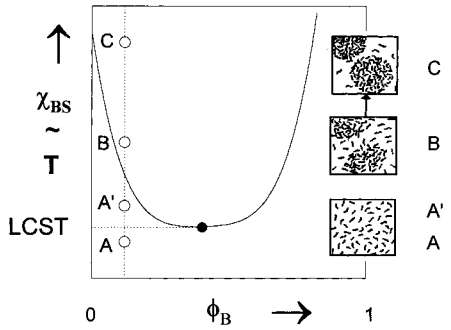

Figure 15. Typical phase diagram for a system "poly(B)/solvent" showing lower critical solution temperature. Starting from the same initial solution, the different states A, A′, B, and C are obtained by increasing the temperature (or χ_{BS}). The resulting microscopic-phase separation, expected in the case of "poly(A)-*g*-poly(B)/S", is sketched on the right axis.

the domain formation is independent of the separation level, either meso- or macroscopic, and that all the self-assembling process can be roughly described on the basis of the thermodynamic behavior of PEO. Only three parameters, $\chi_{BS} = f(T)$, N_B, and ϕ_B (the weight fraction of PEO in the whole solution), are needed to give a quantitative picture of the microdomain formation induced by heating, as sketched in Figure 15.

Considering now the χ_{AS} parameter, which is related to the affinity of the water-soluble backbone for the aqueous medium, we can say that it plays an important role in the stabilization of the two-phase separated system. As qualitatively depicted in eq 17, the swelling of the backbone will affect the microdomain formation and especially the number of PEO side chains per micelle. Varying χ_{AS}, important effects are expected: (1) at very high salt concentration, when Θ conditions are reached. This is the case reported in our experiments; (2) at very low salt concentration with the screening of the electrostatic repulsions. This is out of our conditions, $[K_2CO_3] < 5.5\%$ (w/w).

Generally an increase of the aggregation number is expected when the electrostatic interactions are screened (increase of the ionic strength) or when the solvent quality becomes poorer for the backbone.

Concerning the last parameter χ_{AB}, taking into account the WSB/PEO interactions, we can mention that according to the sharp interface evidenced by SANS in the so-called strong segregation regime (at high temperature and/or salt concentration), a high incompatibility is expected between the two polymer components. Although the χ_{AB} parameter is generally absent from most of the theoretical treatments, the mutual incompatibility between A and B blocks is essential for micellization. Otherwise the incompatibility of the solvent for the polymer blocks will merely give rise to a macroscopic phase separation.

Nevertheless, for multiblocks or polysoaps in selective solvents, the general picture for a micelle is that of a core region consisting of pure B blocks surrounded by a dilute corona of solvated A sequences. Consequently, the interfacial tension, as well as the level of segregation, can be approximated to be that of B blocks in the pure "solvent". We do in fact exactly the same when comparing the microphase separation in WSB-*g*-PEO/water systems with the pseudobinary-phase diagram of PEO in aqueous solutions.

This schematic description of the microphase separation can also be used as a basis to comment on the viscoelastic properties of the associative systems.

It is well-known now that, in semidilute conditions, aqueous solutions of PEO grafted copolymers start to exhibit associative properties as soon as the critical temperature of the PEO/water system is reached. In this weak segregation regime, PEO side chains begin to self-assemble, forming loose clusters which behave as physical cross-links. Any further increase of the temperature above T_{assoc}, will give rise to a strengthening of the microdomains until the so-called strong segregation regime. Using the phase diagram given in Figure 15, this continuous process can be depicted by (1) an increasing number of PEO participating to the microdomains and (2) an increasing concentration inside the PEO micelles.

From a viscoelastic point of view, these two effects result in an increase of both characteristic parameters: the number of elastically active chains of the physical network and the lifetime of the stickers. To qualitatively support the discussion, we can use here the relation issuing from the theory of transient networks, first elaborated by Green and Tobolsky:[65]

$$\eta_0 = \nu_0 kT\tau_x = G_0\tau_x \qquad (20)$$

with η_0 the shear viscosity at zero shear rate, G_0 the linear elastic modulus of an affine network made up of ν_0 elastically active chains, and τ_x the relaxation time of the network which is, in the present context, the reciprocal of the PEO graft disengagement rate from the micelle.

As mentioned above, when the temperature is increased beyond the critical conditions, both ν_0 and τ_x, and consequently η_0, increase.

This is clearly evidenced by the initial slope of the thermothickening curve $\eta = f(T)$, as well as by the shear-thining character of the solution which is expected to arise as soon as τ_x becomes higher than the characteristic experimental time τ_{exp} (inversely proportional to the shear rate).[40] As a matter of fact, above these conditions ($\tau_x > \tau_{exp}$) the transient network is affected by the mechanical shear. In our systems, this effect is responsible for the smoothing of the curve $\eta = f(T)$ with a bell-shaped curvature. At least two different hypotheses can be put forward to explain this dynamic behavior: (1) The PEO grafts snap under shear from hydrophobic clusters faster than they can re-engage. (2) the PEO grafts, pulled out from the microdomains under shear, recombine themselves preferentially into intramolecular clusters.

SANS studies reported here have shown that the bell-shaped signature observed on the $\eta = f(T)$ curves was purely a dynamic phenomenon that cannot be observed on solutions at rest. Complementary experiments under shear will be useful in the future to clearly understand this behavior.

Of course, all the relations existing between the primary structure, the microphase separation behavior, and the viscoelastic properties of the associative systems are not yet perfectly understood. Nevertheless, the most important conclusion that we can draw here is that this quite exhaustive study, performed on PEO grafted copolymers, has permitted us to settle important guidelines which will be helpful to design new responsive systems with predictable properties.

Acknowledgment. Pr. Roland Audebert died during the writing of this paper. Schlumberger Dowell, who actively participated in this scientific story, joins the

coauthors to acknowledge his leadership and pioneer role in the field of thermoassociative polymers. We would like to express our deep gratitude for his guidance and encouragement.

References and Notes

(1) Mantsch, H. H.; Cameron, D. G.; Kartha, V. B. In *Surfactants in solution*; Mittal, K. L., Lindman, B., Eds.; Plenum Press: New York, 1984; Vol. 1.
(2) *Structure and properties in ionomers*; Pinery, M., Eisenberg, A., Eds.; D. Reidel Publishing Co.: Dordrecht, 1987.
(3) *Telechelic Polymers: Synthesis and Applications*; Goethals, E. J., Ed.; CRC Press: New York, 1989.
(4) *Microdomains in Polymer Solutions*; Dubin, P., Ed.; Plenum Press: New York, 1985.
(5) Evani, S.; Rose, G. D. *Polym. Mater. Sci. Eng.* **1987**, *57*, 477.
(6) *Water-soluble polymers, Synthesis, solution properties, and applications*; Shalaby, S. W., McCormick, C. L., Butler, G. B., Eds.; ACS Symposium Series 467; American Chemical Society: Washington DC, 1991.
(7) *Polymers in aqueous media: Performance through association*; Glass, J. D., Ed.; Advances in Chemistry Series 223; American Chemical Society: Washington DC, 1989.
(8) Jenkins, R. D.; Sinha, B. R.; Basset, D. R. *Polym. Mater. Sci. Eng.* **1991**, *65*, 72.
(9) Annable, T.; Ettelaie, R. *Macromolecules* **1994**, *27*, 5616.
(10) Yekta, B. Xu; Duhamel, J.; Adiwidjaja, H.; Winnik, M. A. *Macromolecules* **1995**, *28*, 956.
(11) Hill, A.; Candau, F.; Selb, J. *Prog. Colloid Polym. Sci.* **1991**, *84*, 61.
(12) McCormick, C. L.; Nonaka, T.; Johnson, C. B. *Polymer* **1988**, *29*, 731.
(13) Iliopoulos, I.; Wang, T. K.; Audebert, R. *Langmuir* **1991**, *7*, 617.
(14) Sinquin, A.; Hubert, P.; Dellacherie, E. *Langmuir* **1993**, *9*, 3324.
(15) Tanaka, F.; Edwards, S. F. *J. non-Newtonian Fluid Mech.* **1992**, *43*, 247, 273, and 289.
(16) Borisov, O. V.; Halperin, A. *Langmuir* **1995**, *11*, 2911.
(17) Semenov, A. N.; Joanny, J.-F.; Khokhlov, A. R. *Macromolecules* **1995**, *28*, 1066.
(18) Khalatur, P. G.; Khokhlov, A. R. *Macromol. Theory Simul.* **1996**, *5*, 713 and 749.
(19) Annable, T.; Buscall, R.; Ettelaie, R.; Whittlestone, D. *J. Rheol.* **1993**, *37*, 695.
(20) Wang, T. K.; Iliopoulos, I.; Audebert, R., Chapter 14 of ref 6.
(21) Audebert, R.; Iliopoulos, I.; Hourdet, D. *Polimery* **1997**, *42*, 237.
(22) Thuresson, S.; Nilsson, B.; Lindman, B. *Langmuir* **1996**, *12*, 530.
(23) Bokias, G.; Hourdet, D.; Iliopoulos, I.; Staikos, G.; Audebert, R. *Macromolecules* **1997**, *30*, 8293.
(24) Cabane, B.; Wong, K.; Lindner, P.; Lafuma, F. *J. Rheol.* **1997**, *41*, 531.
(25) Effing, J. F.; Kwak, J. C. T. *Angew. Chem., Int. Ed. Engl.* **1995**, *34*, 89.
(26) Brown, W.; Schillen, K.; Almgren, M.; Hvidt, S.; Bahadur, P. *J. Phys. Chem.* **1991**, *95*, 1850.
(27) Suto, S.; Nishibori, W.; Kudo, K.; Karasawa, M. *J. Appl. Polym. Sci.* **1989**, *37*, 737.
(28) Klug, E. D. *J. Polym. Sci., Part C* **1971**, *36*, 491.
(29) Sarkar, N. *J. Appl. Polym. Sci.* **1979**, *24*, 1073.
(30) Werbowyj, R. S.; Gray, D. S. *Macromolecules* **1980**, *13*, 69.
(31) Carlsson, A.; Karlström, G.; Lindman, B. *Colloids Surf.* **1990**, *47*, 147.
(32) Cabane, B.; Lindell, K.; Engström, S.; Lindman, B. *Macromolecules* **1996**, *29*, 3188.
(33) Loyen, K., Iliopoulos, I.; Audebert, R.; Olsson, U. *Langmuir* **1995**, *11*, 1053.
(34) Hourdet, D.; L'alloret, F.; Audebert, R. *Polym. Prepr. (Am. Chem. Soc., Div. Polym. Chem.)* **1993**, *34*, 972.
(35) Hourdet, D.; L'alloret, F.; Audebert, R. *Polymer* **1997**, *38*, 2535.
(36) Schlumberger Dowell C. Eur. Patent 0 583 814 A1, 1993; 0 629 649 A1, 1994.
(37) *Chem. Eng. News* **1997**, *75*, 26.
(38) Hourdet, D.; L'alloret, F.; Audebert, R. *Polymer* **1994**, *35*, 2624.
(39) L'alloret, F.; Hourdet, D.; Audebert, R. *Colloid Polym. Sci.* **1995**, *273*, 1163.
(40) L'alloret, F.; Maroy, P.; Hourdet, D.; Audebert, R. *Rev. Inst. Fr. Pet.* **1997**, *52*, 117.
(41) Cotton J.-P. In *Neutron, X-ray and light scattering: Introduction to an investigative tool for colloidal and polymeric systems*; Lindner, P., Zemb, T., Eds.; Elsevier Science Publishers B. V.: Amsterdam, 1991; p 3.
(42) Bailey, F. E.; Callard, R. W. *J. Appl. Polym. Sci.* **1959**, *1*, 56.
(43) Roe, R. J.; Fishkis, M.; Chang, J. C. *Macromolecules* **1981**, *14*, 1091.
(44) Shibayama, T.; Tanaka, T.; Han, C. C. *J. Chem. Phys.* **1992**, *97*, 6842.
(45) Shibayama, M.; Tanaka, T. *J. Chem. Phys.* **1995**, *102*, 9392.
(46) Shibayama, M.; Ikkai, F.; Inamoto, S.; Nomura, S.; Han, C. C. *J. Chem. Phys.* **1996**, *105*, 4358.
(47) Schosseler, F.; Moussaid, A.; Munch, J.-P.; Candau, S. J. *J. Phys. II Fr.* **1991**, *1*, 1197.
(48) Borue, V.; Erukhimovitch, I. *Macromolecules* **1988**, *21*, 3240.
(49) De Gennes, P. G.; Pincus, P.; Velasco, R. M.; Brochard F. *J. Phys.* **1976**, *37*, 1461.
(50) Essafi, W.; Lafuma, F.; Williams, C. E. In *Macro-ion characterization. From dilute solutions to complex fluids*; Schmitz, K. S., Ed.; ACS Symposium Series 548; American Chemical Society: Washington DC, 1994; p 278.
(51) Porod, G. *Kolloid Z. Polym.* **1951**, *124*, 83; **1952**, *51*, 109.
(52) Liu, K. J.; Parsons, J. L. *Macromolecules* **1969**, *2*, 529.
(53) Maconnachie, A.; Vasudevan, P.; Allen, G. *Polymer* **1978**, *19*, 33.
(54) Hager, S. L.; Macrury, T. B. *J. Appl. Polym. Sci.* **1980**, *25*, 1559.
(55) Kjellander, R.; Florin-Robertsson, E. *J. Chem. Soc., Faraday Trans. 1* **1981**, *77*, 2053.
(56) Graham, N. B.; Zulfiqar, M.; Nwachuku, N. E.; Rashid, A. *Polymer* **1989**, *30*, 528.
(57) Nagarajan, R.; Ganesh, K. *J. Chem. Phys.* **1989**, *90*, 5843.
(58) De Gennes, P. G. In *Solid state physics*; Liebert, L., Ed.; Academic Press: New York, 1977; Suppl. 14, p 1.
(59) Leibler, L.; Orland, H.; Wheeler, J. C. *J. Chem. Phys.* **1983**, *79*, 3550.
(60) Noolandi, J.; Hong, M. H. *Macromolecules* **1983**, *16*, 1443.
(61) Halperin, A. *Macromolecules* **1987**, *20*, 2943.
(62) Bahadur, P.; Sastry, N. V.; Marti, S.; Riess, G. *Colloid Surf.* **1985**, *16*, 337.
(63) Khougaz, K.; Astafieva, I.; Eisenberg, A. *Macromolecules* **1995**, *28*, 7135.
(64) Procházka, O.; Tuzar, Z.; Kratochvíl, P. *Polymer* **1991**, *32*, 3038.
(65) Green, M. S.; Tobolsky, A. V. *J. Chem. Phys.* **1946**, *14*, 80.

MA980220L